Radiation characteristics of detached divertor plasmas in W7-X

E. Wang[a,*], R. König[b], M. Krychowiak[b], S. Brezinsek[a], P. Drews[a], D. Gradic[b], M. Jakubowski[b], P. Kornejew[b], T. Kremeyer[b], C. Killer[b], Y. Liang[a], O. Neubauer[a], A. Pandey[b], L. Rudischhauser[b], S. Sereda[c], G. Schlisio[b], S. Xu[a], and the W7-X team

[a]*Institut für Energie- und Klimaforschung – Plasmaphysik, Forschungszentrum Jülich GmbH, Partner of the Trilateral Euregio Cluster (TEC), Jülich, Germany*

[b]*Max-Planck-Institut für Plasmaphysik, Greifswald, Germany*

[c]*University of Wisconsin-Madison, Madison WI, USA*

**Correspoding author.*

E-mail address: e.wang@fz-juelich.de

Abstract

Detached divertor plasmas has been achieved by density ramp in W7-X. During the transition into detachment, the main divertor radiation region moves from the region close to the divertor targets to the region around LCFS. The typical spatial distributions of carbon and hydrogen Balmer lines in detached divertor plasma are presented. They show that the line emissions of CH produced by chemical sputtering is still strong close to the targets. The C I fills up the whole detached divertor plasma and its intensity increases when approaching the targets due to the dissociation from hydrocarbon and self-sputtering. The C II and C III are mainly located at around LCFS region. Meanwhile, the distribution of hydrogen Balmer lines is considerably flatter in detached divertor plasma. The Balmer line ratios indicate that the detached divertor plasma seems to be still in excitation or partial recombination state. This is consistent with the divertor Langmuir probe measurements which shows that the electron temperature near strike line is around 6 eV. Finally, the electron pressure at upstream and downstream position is measured and its ratio shows that the electron pressure drops significantly along the magnetic field lines. However, the pressure can not drop further due to the lack of the volume recombination in detached divertor plasma.

Keywords: detached divertor plasmas; radiation distribution; electron pressure; W7-X

1. Introduction

In the fusion devices, detached divertor plasma is an attractive operational scenario to reduce the energy and particles reaching the target tiles [1]. The basic physical feature of the detached plasma is that the total plasma pressure along the magnetic field lines has large gradients compared to the high recycling regime. And the large ionization losses and impurity radiation in the divertor lead to low electron temperatures which allow volume recombination (T_e < 1.5 eV) processes to take place [2]. The combination of plasma pressure reduction and the hydrogen volume recombination results in the lower incident ion fluxes to the divertor plates. A further beneficial effect of the detached divertor plasma is that the largest particle flux impinging on the targets is in the form of neutral atoms and molecules which can not be accelerated by the sheath potential. This minimizes the erosion on the divertor targets produced by the physical sputtering [3].

The detached divertor plasma has been widely investigated in many tokamaks and stellarators by using spectroscopy diagnostics [2], [4]–[6]. It is found that the main radiation region in detachment is located at around the X-point and the hydrogen recombination region expands from the target surface to the most of divertor plasma. In experiments, the evidence for volume recombination is usually obtained from the increase in the ratio of the Balmer series, e.g. H_γ/H_α intensity ratio.

W7-X is a large advanced stellarator which aims at long stable steady state operation with high plasma performance. Therefore, reducing the power and particles onto the targets, especially in the long stable steady state discharges, and reducing the target erosion is a critical issue. In Operation Phase 1.2 (OP1.2), W7-X run in island divertor configurations with ten divertor units made of graphite. Stable detachment scenarios have been achieved, in which the power loads on divertor plates was reduced by up to a factor of ten [7], [8]. In OP1.2(b), three boronizations for wall conditioning were applied, which resulted in strong decrease of oxygen content in the plasma with carbon remaining the main intrinsic radiation source [9]. Here, we report on the spatial distributions of CH, C I, C II and C III in the detached divertor plasma. In addition, the spatial distributions of line emissions from hydrogen molecules and atoms are presented and their Balmer line ratios are used to indicate the degree of volume recombination in the detached divertor plasma. Finally, the electron pressure on the upstream and downstream is measured and the pressure along the magnetic fields is investigated.

2. Experimental setup

W7-X is a large advanced stellarator with a major radius R = 5.5 m and a minor radius a ~ 0.5 m. There are total 50 non-planar and 20 planar superconducting coils to produce the main magnetic field structure with island chains (ι = n/m = 5/6, 5/5, and 5/4) in the edge. The configuration featuring ι=5/5 island is called standard divertor configuration, while the other two are referred to as low- and high- ι divertor configurations. A detailed description of the magnetic configurations in W7-X can be found in [10]. In order to measure the divertor plasma radiation, several divertor spectrometers have been installed to observe the divertor plasma. Fig.1 shows the field of view of two spectrometer systems which were installed in machine half-module HM51 [11]. One was the horizontal line of sights which were adjusted parallel to the horizontal divertor plate and onto the middle nozzle (out of five) of the divertor gas injection system. It comprised 27 viewing chords separated by ~5 mm in the minor radial direction. The emissions from the divertor plasma were transmitted through 27 optical fibers with a core diameter of 150 µm to a Czerny-Turner spectrometer (Teledyne Princeton Instruments: SP2750). Its focal length was 750 mm and three gratings (300, 1200 and 2400 g/mm) were installed. Its detector was a frame transfer CCD camera (Teledyne Princeton Instruments: ProEM HS:1024B) with 1024 × 1024 pixels (pixel size: 13 × 13 µm). The spectral resolution was $\Delta\lambda_{FWHM}$ = 0.23, 0.06 and 0.03 nm at 435.8 nm with an entrance slit width W_{slit} = 50 µm. The other one was the tangential line of sight which covered the most of the divertor plasma. The emissions were transmitted through the divertor spectroscopy endoscope installed at the port AEJ51 and additional optical fibers (core diameter: 800 µm) to an overview spectrometer. This spectrometer had five built-in compact Czerny-Turner spectrometers (Avantes: ULS2048L) which were equipped with 1800, 1800, 1800, 1200 and 830 g/mm gratings, respectively. The measured wavelength ranges were 300 - 455 nm, 454 – 584 nm, 583 – 685 nm, 684 – 886 nm and 885 - 1100 nm.

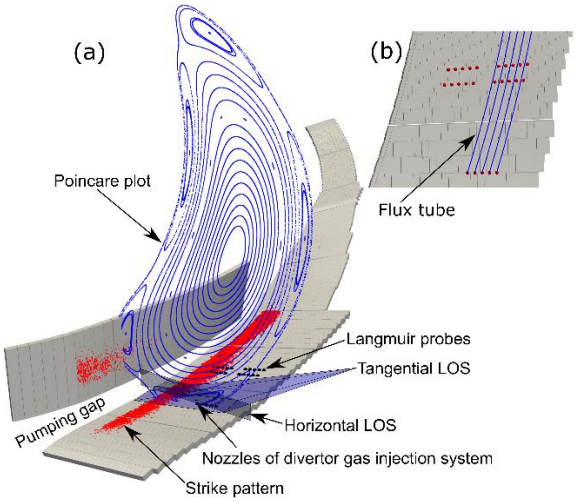

Fig.1 (a) Line of sights of divertor spectrometers in machine half-module HM51. The Poincare plot shows the magnetic field structure in the standard divertor configuration. (b) Top view of the magnetic field lines tracing from the nozzles of divertor gas injection system to the divertor Langmuir probes.

In the horizontal divertor plate in machine module HM51, a divertor gas injection system with five nozzles was installed as shown in Fig.1. This divertor gas injection system was also used for thermal helium beam diagnostic measurements. The magnetic field connection length in standard divertor configuration at this poloidal cross section is shown in Fig.2. The radial distance between the last closed flux surface (LCFS) and the horizontal divertor plate was ~ 9 cm. There were 20

Langmuir probes installed nearby the nozzles of the divertor gas injection system [12]. The first five Langmuir probes were located nearly at the same flux tubes tracing from the five nozzles of divertor gas injection system as shown in Fig.1(b). The radial distance between the flux tubes and the first five Langmuir probes is about 1-2 cm. In addition, a multi-purpose manipulator (MPM) was installed at the upstream to measure the edge plasma parameter profiles [13].

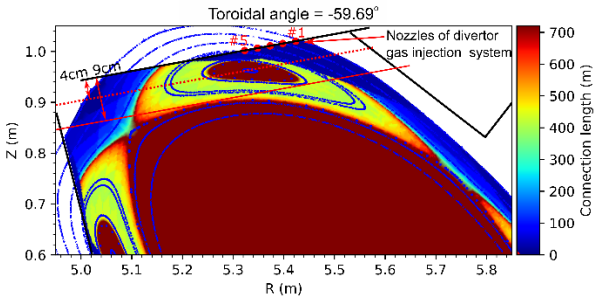

Fig.2 Connection length of magnetic field lines in standard divertor configuration.

3. Experimental results

3.1 Spatial distributions of line emissions

In W7-X, stable detached discharges have been achieved in OP1.2 by H_2 gas fueling using the main gas injection system, H_2 pellet injection, divertor H_2 gas injection and impurity gas seeding (e.g. N_2 and Ne). Fig. 3 shows time traces of a detached discharge achieved by ramping up plasma radiation in a feedback loop using H_2 fueling with the nozzle #4 of the divertor gas injection system in HM51. With increasing plasma density, the radiation fraction ramped to more than 80%, which resulted in a very low level of particle and heat fluxes on the divertor plates. At t = 4 s, the ECRH power decreased from P_{ECRH} = 6 MW to 3 MW and the detachment lasted until the end of the discharge without any further fueling. In this discharge, the radiation was mainly from the carbon. With density ramping-up, the temperature in the divertor plasma decreased, which resulted in the C II and C III moving from the region near to the divertor targets (d < 4 cm) in attachment to the region close to the LCFS ($d_{LCFS} \approx 9$ cm) in detachment. This phenomenon was also descripted in reference [14]. For the CH molecules dissociated from hydrocarbon and produced by chemical sputtering, it was always located near to the divertor targets. While the C I filled up the whole divertor plasma and its intensity increased when approaching the divertor targets as shown in Fig.5(b). This means that the hydrocarbon made a significantly contribution to the C I emission near to divertor plates in addition to the carbon self-sputtering. The hydrogen Balmer lines and molecule Fulcher band lines (Fulcher band spectrum measured in W7-X could be found in reference [15]) indicate that the neutral hydrogen atoms and molecules distribute all over the whole divertor plasma in detachment as shown in Fig.4(b) and Fig.5(a). Here, the spatial distributions of H_2 Fulcher and C I line emissions shown in Fig.5 are from different detached discharges, however, their spatial distributions were similar as discharge #20181010.033.

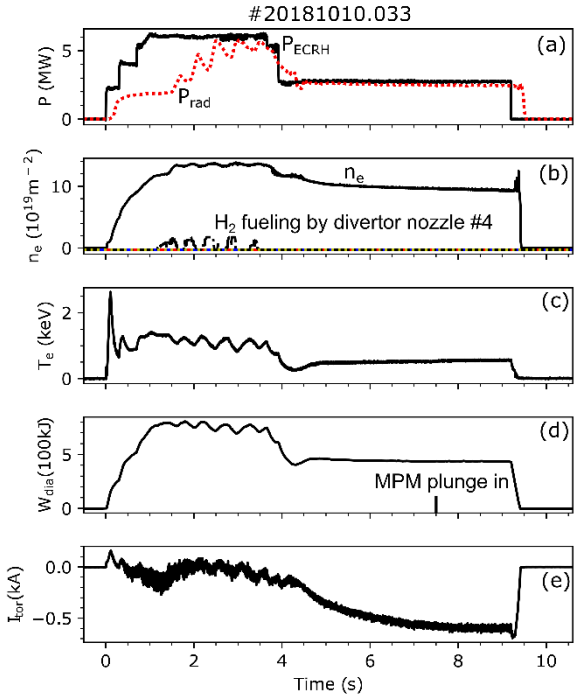

Fig.3 Time traces of a representative detached discharge #20181010.033. (a) ECRH heating power and radiated power, (b) line integrated electron density and H_2 gas injection by the nozzle #4 of divertor gas injection system installed in HM51, (c) core electron temperature, (d) diamagnetic energy; MPM plunge in at t=7.5 s, and (e) toroidal plasma current.

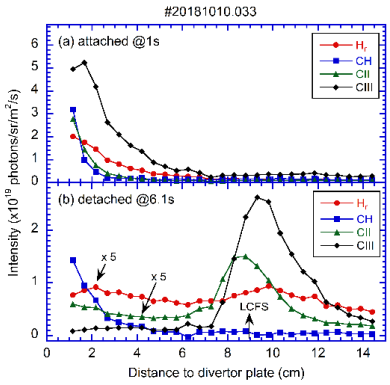

Fig.4 Radial profiles of LOS integrated spectral line emission H_γ (434.0 nm), CH Gerö band (431.0 nm), C II (426.8 nm) and C III (465.0 nm) in (a) attached and (b) detached divertor plasma.

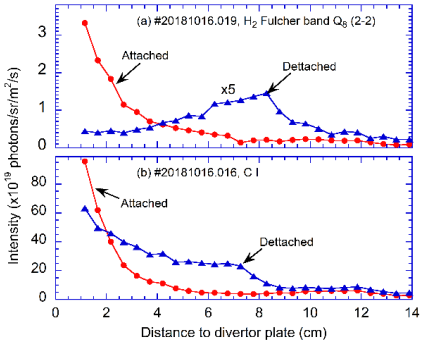

Fig.5 Radial profiles of LOS integrated spectral line emission H_2 Fulcher band Q_8 (2-2) and C I (909.5nm) in attached and detached divertor plasma.

3.2 Spectroscopic determination of ionization state

The brightness of spectrums for various elements was calculated using a collisional-radiative model by ADAS [16]. For example, the emissivity of H_β (n=4→ n=2) is written as:

$$\epsilon_{4\to2} = n_e n_H^{0+} PEC^{exc}(n_e, T_e) + n_e n_H^{1+} PEC^{rec}(n_e, T_e)$$

The PECs are the so-called photon emissivity coefficients for excitation and recombination which have been calculated for hydrogen in ADAS. The PEC^{exc} and PEC^{rec} of H_β are illustrated in Fig.6 for three different densities (here the Open-ADAS data file was used: pec12#h_pju#h0.dat). It can be seen that the recombination process dominates in the plasma when T_e < 1.5 eV while ionization process dominates when T_e > 1.5 eV. If only recombination or ionization process is considered, the line emission ratio of H_γ (n=5→n=2) and H_β (n=4→n=2) is written as:

$$\frac{\epsilon_{5\to2}}{\epsilon_{4\to2}} = \frac{PEC_{H_\gamma}^{rec}}{PEC_{H_\beta}^{rec}} \quad \text{and} \quad \frac{\epsilon_{5\to2}}{\epsilon_{4\to2}} = \frac{PEC_{H_\gamma}^{exc}}{PEC_{H_\beta}^{exc}}$$

Fig.7 shows H_γ/H_β and H_δ/H_γ ratios for three different densities. These line ratios depend weakly on the electron density in the high electron temperature (T_e > 5 eV), while strongly on the electron temperature and density in the low electron temperature (T_e < 5 eV), especially the recombination dominate region (T_e < 1.5 eV).

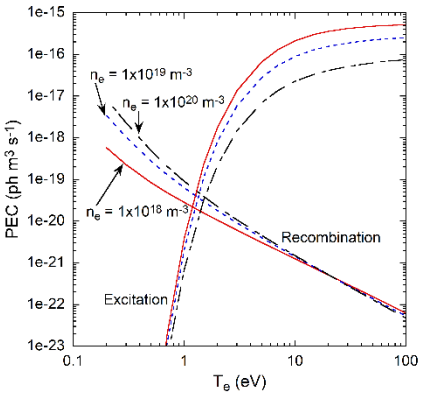

Fig.6 Photon emission coefficient (PEC) of H_β for excitation and recombination at electron density n_e = 1 x 10^{18} m^{-3}, 1 x 10^{19} m^{-3} and 1 x 10^{20} m^{-3}.

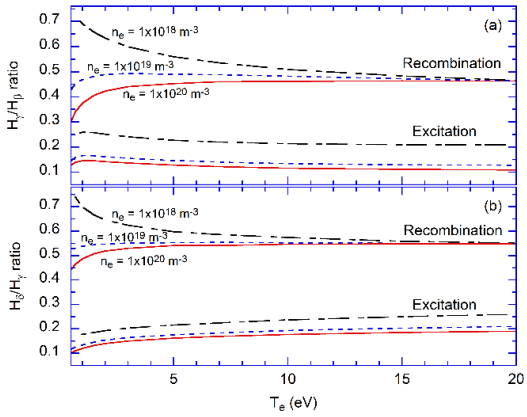

Fig.7 Intensity ratios of (a) H_γ/H_β and (b) H_δ/H_γ, calculated using ADAS photon emissivity coefficients (pec12#h_pju#h0.dat) for recombining and ionizing plasma component at electron density n_e= 1 x 10^{19} m^{-3}, 1 x 10^{19} m^{-3}, and 1 x 10^{20} m^{-3}.

The spatial distributions of hydrogen Balmer lines and their line ratios have been measured in attached and detached divertor plasma. In attached divertor plasma, H_γ and H_δ mainly come from the region close to the target surface as shown in Fig.8(a). The spatial distance to divertor plates is smaller than 3 cm and the H_δ/H_γ ratio increases when approaching targets. While in detachment, H_γ and H_δ line emission profile is roughly flat and the H_δ/H_γ ratio is around 0.24 in the most of divertor plasma. Fig.9 shows H_γ/H_β and H_δ/H_γ ratios measured by the overview spectrometer, the line of sight of which covered nearly the whole divertor plasma. The values of H_γ/H_β and H_δ/H_γ are around 0.26 and 0.35 after 4.5s. By comparing the measurements and the ADAS calculation shown in Fig.7, it seems that the detached divertor plasma is still in excitation or partial recombination state.

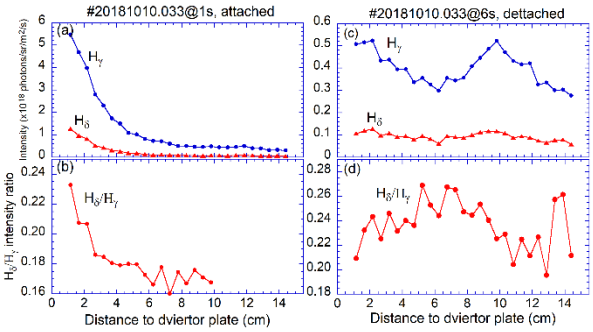

Fig.8 Intensity profiles of H_γ and H_δ and their line ratio. (a) and (b) attached case; (c) and (d) detached case.

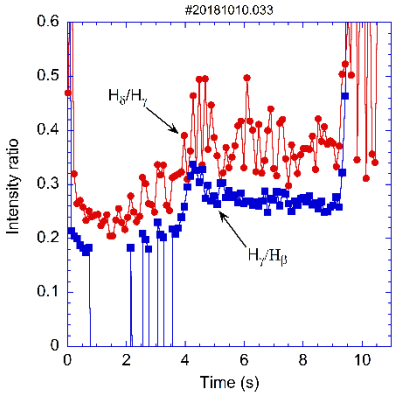

Fig.9 Intensity ratios of H_δ/H_γ and H_γ/H_β measured by divertor overview spectrometer which integrated most of the divertor plasma.

3.3 Degree of detachment (DOD)

Plasma detachment is characteristic as a significant loss of the energy, momentum and particle flux parallel to the magnetic field lines from the upstream to the downstream. The degree of detachment (DOD) could be determined by the comparison of the upstream and downstream plasma measurements. Here we focus on the electron pressure and compare its upstream and downstream measurements as discussed in reference [17], [18].

Fig.10(b) shows the electron density and temperature profiles measured by the HM51 divertor Langmuir probes during detachment. The location of the probes and the magnetic structure is shown in Fig.10(a). The electron temperature near strike line is still around 6 eV which is much higher than the recombination dominated domain of $T_e < 1.5$ eV, and the electron density is 4.8 x 10^{18} m^{-3} in detachment. At the upstream position, the electron temperature and density profiles were measured by the midplane MPM. The HM51 divertor Langmuir probes are projected to the MPM poloidal cross section and their positions are shown in Fig.11(a). It shows that the Langmuir probe #6 was the closest one to the path of MPM, where the electron temperature and density at the upstream was 14 eV and 7 x 10^{18} m^{-3}, respectively. Therefore, the electron pressure ratio between the upstream and the downstream along this flux tube is:

$$\frac{p_e^t}{p_e^u} = \frac{2n_e^t T_e^t}{n_e^u T_e^u} = \frac{2 \times 3.5 \times 10^{18} \times 3}{7 \times 10^{18} \times 14} = 0.21$$

It shows a significantly drop of the electron pressure along this magnetic tube due to the detachment, although this magnetic tube is a little far away from LCFS. In tokamak, this ratio could reach much smaller, e.g. ≈ 0.04 ($T_e \approx 1.5$ eV) in the volume recombination detachment in Alcator C-Mod [17], [18]. In W7-X, the edge magnetic topology is quite different from the tokamaks, which results in the transport along and perpendicular to the magnetic field is much complicated [19]. From the above typical detachment discharges in W7-X, it seems that the downstream electron pressure can not drop any more due to the lack of volume recombination.

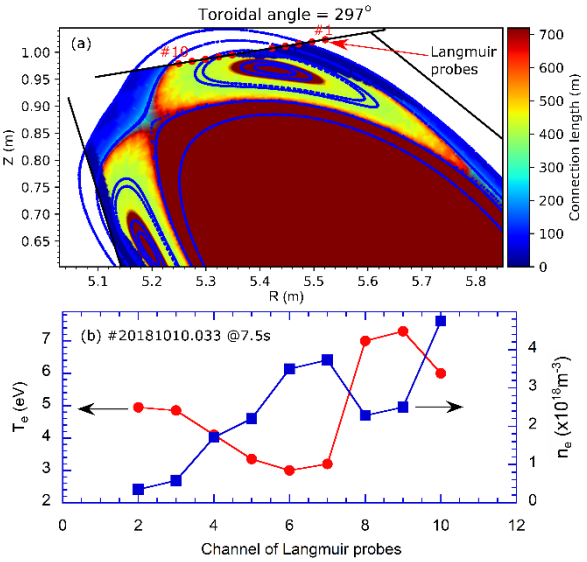

Fig.10 (a) Connection length and Poincare plot of magnetic field lines (standard divertor configuration) at the poloidal cross-section of Langmuir probes. (b) Electron density and temperature profiles measured by divertor Langmuir probes in detached plasma.

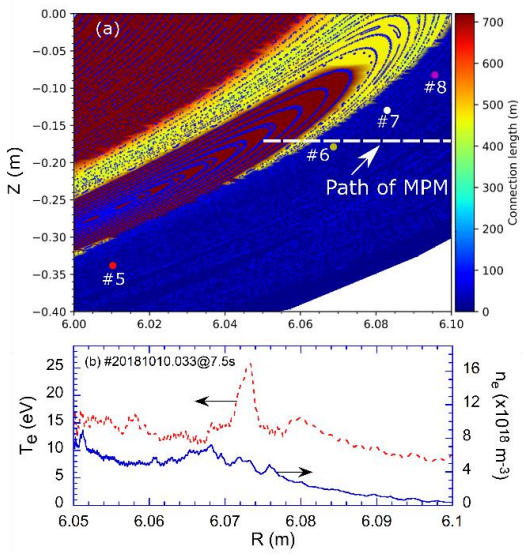

Fig.11 (a) Scheme of the path of mid-plane MPM. The connection length and Poincare plot are the standard divertor magnetic configuration. The HM51 divertor Langmuir probe #5, #6 #7 and #8 are projected to the MPM cross section. (b) Electron density and temperature profiles at upstream measured by MPM.

4. Summary

In W7-X, the spatial distributions of line emissions have been obtained in attached and detached divertor plasma. They show that C II and C III mainly come from the region near to the LCFS, while the C I fully fills in the whole divertor plasma and its intensity increases when approaching to the divertor plates. CH produced by chemical sputtering is still located at the region close to the divertor plates. It means that the physical sputtering produced by hydrogen nearly disappears due to the low temperature in detachment and the carbon source at divertor targets is mainly produced by chemical sputtering in addition to the carbon self-sputtering. In addition, the hydrogen molecule and atom lines distribute roughly flat in the whole divertor volume instead of only locate at the target surface in attachment. The hydrogen Balmer line ratios indicate that the detached divertor plasma seems still in excitation or partial recombination state. This is consistent with the divertor Langmuir probe measurements which shows that the electron temperature near the strike line is about 6 eV. This temperature is much higher than the recombination dominated temperature, i.e. < 1.5 eV. Meanwhile, the electron pressure between upstream and downstream is compared. The electron pressure ratio along one magnetic field line in scrape-off layer is 0.21 which can not be further smaller due to the lack of volume recombination.

Acknowledgements

This work has been carried out within the framework of the EUROfusion Consortium, funded by the European Union via the Euratom Research and Training Programme (Grant Agreement No 101052200 — EUROfusion). Views and opinions expressed are however those of the author(s) only and do not necessarily reflect those of the European Union or the European Commission. Neither the European Union nor the European Commission can be held responsible for them.

References

[1] A. W. Leonard, “Plasma detachment in divertor tokamaks,” *Plasma Physics and Controlled Fusion*, vol. 60, no. 4, p. 044001, Feb. 2018, doi: 10.1088/1361-6587/AAA7A9.

[2] D. Lumma, J. L. Terry, and B. Lipschultz, "Radiative and three-body recombination in the Alcator C-Mod divertor," *Physics of Plasmas*, vol. 4, no. 7, p. 2555, Sep. 1998, doi: 10.1063/1.872234.

[3] D. G. Whyte *et al.*, "The effect of detachment on carbon divertor erosion/redeposition in the DIII-D tokamak," *Nuclear Fusion*, vol. 41, no. 9, p. 1243, Sep. 2001, doi: 10.1088/0029-5515/41/9/313.

[4] A. Loarte *et al.*, "Plasma detachment in JET Mark I divertor experiments," *Nuclear Fusion*, vol. 38, no. 3, p. 331, Mar. 1998, doi: 10.1088/0029-5515/38/3/303.

[5] U. Wenzel, K. Behringer, A. Carlson, J. Gafert, B. Napiontek, and A. Thoma, "Volume recombination in divertor I of ASDEX Upgrade," *Nuclear Fusion*, vol. 39, no. 7, p. 873, Jul. 1999, doi: 10.1088/0029-5515/39/7/304.

[6] N. Ramasubramanian *et al.*, "Characterization of the island divertor plasma of W7-AS stellarator in the deeply detached state with volume recombination," *Nuclear Fusion*, vol. 44, no. 9, p. 992, Aug. 2004, doi: 10.1088/0029-5515/44/9/008.

[7] M. Jakubowski *et al.*, "Overview of the results from divertor experiments with attached and detached plasmas at Wendelstein 7-X and their implications for steady-state operation," *Nuclear Fusion*, vol. 61, no. 10, p. 106003, Aug. 2021, doi: 10.1088/1741-4326/AC1B68.

[8] D. Zhang *et al.*, "First Observation of a Stable Highly Dissipative Divertor Plasma Regime on the Wendelstein 7-X Stellarator," *Physical Review Letters*, vol. 123, no. 2, p. 025002, Jul. 2019, doi: 10.1103/PHYSREVLETT.123.025002/FIGURES/5/MEDIUM.

[9] S. Sereda *et al.*, "Impact of boronizations on impurity sources and performance in Wendelstein 7-X," *Nuclear Fusion*, vol. 60, no. 8, p. 086007, Jul. 2020, doi: 10.1088/1741-4326/AB937B.

[10] J. Geiger, C. D. Beidler, Y. Feng, H. Maaßberg, N. B. Marushchenko, and Y. Turkin, "Physics in the magnetic configuration space of W7-X," *iopscience.iop.org*, p. 014004, 2015, doi: 10.1088/0741-3335/57/1/014004.

[11] E. Wang, S. Brezinsek, S. Sereda, … B. B.-P., and undefined 2020, "Impurity sources and fluxes in W7-X: from the plasma-facing components to the edge layer," *iopscience.iop.org*, Accessed: May 20, 2022. [Online]. Available: https://iopscience.iop.org/article/10.1088/1402-4896/ab4c04/meta

[12] L. Rudischhauser, M. Endler, U. Höfel, K. C. Hammond, J. P. Kallmeyer, and B. D. Blackwell, "The Langmuir probe system in the Wendelstein 7-X test divertor," *Review of Scientific Instruments*, vol. 91, no. 6, p. 063505, Jun. 2020, doi: 10.1063/1.5143013.

[13] P. Drews *et al.*, "Operation of probe heads on the Multi-Purpose-Manipulator at W7-X in OP 1.2a," *Fusion Engineering and Design*, vol. 146, pp. 2353–2355, Sep. 2019, doi: 10.1016/J.FUSENGDES.2019.03.188.

[14] M. Krychowiak *et al.*, "Gaussian Process Tomography of carbon radiation in the transition to detached plasmas in the Wendelstein 7-X stellarator," *pure.mpg.de*, Accessed: May 31, 2022. [Online]. Available: https://pure.mpg.de/rest/items/item_3358472/component/file_3358473/content

[15] E. Wang *et al.*, “Spectroscopic study of hydrogen particle behaviour in island divertor of W7-X,” *pure.mpg.de*, Accessed: Jun. 14, 2022. [Online]. Available: https://pure.mpg.de/rest/items/item_3359046/component/file_3359047/content

[16] W. Han *et al.*, “Ionization state, excited populations and emission of impurities in dynamic finite density plasmas: I. The generalized collisional–radiative model for light elements,” *Plasma Physics and Controlled Fusion*, vol. 48, no. 2, p. 263, Jan. 2006, doi: 10.1088/0741-3335/48/2/007.

[17] B. LaBombard *et al.*, “Experimental investigation of transport phenomena in the scrape-off layer and divertor,” *Journal of Nuclear Materials*, vol. 241–243, pp. 149–166, Feb. 1997, doi: 10.1016/S0022-3115(97)80037-2.

[18] B. LaBombard *et al.*, “Scaling and transport analysis of divertor conditions on the Alcator C-Mod tokamak,” *Physics of Plasmas*, vol. 2, no. 6, p. 2242, Jun. 1998, doi: 10.1063/1.871248.

[19] Y. Feng, M. Kobayashi, T. Lunt, and D. Reiter, “Comparison between stellarator and tokamak divertor transport,” *Plasma Physics and Controlled Fusion*, vol. 53, no. 2, p. 024009, Jan. 2011, doi: 10.1088/0741-3335/53/2/024009.